Scalable and ultralow power silicon photonic two-dimensional phased array 🄵

Michelle Chalupnik ✉ 🄳 ; Anshuman Singh 🄳 ; James Leatham 🄳 ; Marko Lončar; Moe Soltani ✉ 🄳

⊕ Check for updates

CrossMark

🌐 View Online

📄 Export Citation

Articles You May Be Interested In

Cascaded domain engineering optical phased array for beam steering

Appl. Phys. Rev. (August 2023)

On a Variable Transformation Between Two Integrable Systems: The Discrete Hungry Toda Equation and the Discrete Hungry Lotka-Volterra System

AIP Conference Proceedings (September 2010)

Genetic similarity analysis of *Rhynchostylis retusa* (L.) Blume orchids using OPA 15 and OPA 03 RAPD marker

AIP Conference Proceedings (October 2018)

AIP Publishing

Scalable and ultralow power silicon photonic two-dimensional phased array ⒡

View Online   Export Citation   CrossMark

Michelle Chalupnik,[1,2,3,a] ⒾⒹ **Anshuman Singh,**[1] ⒾⒹ **James Leatham,**[4] ⒾⒹ **Marko Lončar,**[5] **and Moe Soltani**[1,a] ⒾⒹ

AFFILIATIONS

[1] Raytheon BBN, 10 Moulton Street, Cambridge, Massachusetts 02138, USA
[2] Department of Physics, Harvard University, Cambridge, Massachusetts 02138, USA
[3] Currently with Aliro Quantum, Brighton, Massachusetts 02135, USA
[4] Raytheon Intelligence and Space, 2000 El Segundo Dr., El Segundo, California 90245, USA
[5] John Paulson School of Engineering and Applied Science, Harvard University, Cambridge, Massachusetts 02138, USA

[a] Authors to whom correspondence should be addressed: mo.soltani@raytheon.com and michelle.chalupnik@raytheon.com

ABSTRACT

Photonic integrated circuit based optical phased arrays (PIC-OPAs) are emerging as promising programmable processors and spatial light modulators, combining the best of planar and free-space optics. Their implementation on silicon photonic platforms has been especially fruitful. Despite much progress in this field, demonstrating steerable two-dimensional (2D) OPAs that are scalable to a large number of array elements and operate with a single wavelength has proven a challenge. In addition, the phase shifters used in the array for programming the far-field beam are either power hungry or have a large footprint, preventing the implementation of large scale 2D arrays. Here, we demonstrate a two-dimensional silicon photonic phased array with high-speed (~330 kHz) and ultralow power microresonator phase-shifters with a compact radius (~3 μm) and 2π phase shift ability. Each phase-shifter consumes an average of ~250 μW of static power for resonance alignment and ~50 μW of power for far-field beamforming, a more than one order of magnitude improvement compared to prior OPA works based on waveguide-based thermo-optic phase shifters. Such PIC-OPA devices can enable a new generation of compact and scalable low power processors and sensors.

INTRODUCTION

Integrated optical phased arrays (OPAs) in a silicon photonic integrated circuit (PIC) platform are a form of on-chip programmable spatial light modulators (SLMs) and have shown great promise for a broad range of applications, including holography, light detection and ranging (LiDAR), and free-space communications.[1–4] PIC-OPAs can enable the formation of complex beam patterns as well as precise and high speed beam steering for LiDAR or sensing. As compact and high-speed programmable SLMs, PIC-OPAs promise a new generation of advanced on-chip optical processor engines[5–7] that can replace existing devices and their associated bulky components.[8]

Despite significant advancements in PIC-OPA technology, most demonstrated works rely on waveguide phase shifters, which are either power hungry or have large footprints,[9–16] inhibiting the scalability of two-dimensional (2D) phased arrays to larger numbers of array elements. The majority of 2D beamforming and beam steering work using PICs relies on tuning the input laser for steering in one direction and programming the phase shifters for steering in the other orthogonal direction (e.g., Refs. 3, 10, 12, 16, and 17). Some other 2D phased array works place phase shifters outside the array; however, these approaches do not show scalability due to their optical routing topology limitations[11,15] and experience larger optical insertion losses for larger arrays.[15] 2D phased arrays based on MEMS[14] have been demonstrated with promising results. However, the required large voltage (~10 V) for the MEMS components and the custom nature of device fabrication make these devices incompatible with CMOS driving circuits as well as CMOS manufacturing. The recent interesting work in Ref. 6 designs and employs an array of silicon photonic crystal (PC) cavities for making a 2D SLM, wherein each PC cavity acts simultaneously as a phase shifter and

an antenna.[6] However, each cavity that is tuned optically with a different wavelength provides a maximum phase shift of 0.2π, limiting the full range of phase programming. In addition, the entire PC layer is suspended, which limits the maximum power that each cavity can handle before transitioning to thermal and absorption nonlinearity regimes.

Recently, silicon ring resonator phase shifters have proven to be a solution for small footprint and low power consumption phase shifters in optical phased arrays, allowing a path for phased array scalability.[18] When these resonators are designed in the strong overcoupling regime, they can provide a phase shift of 2π for their corresponding antenna with low power consumption. Optical phased arrays with silicon ring resonator phase shifters are also relatively robust and can be fabricated reproducibly in standard CMOS foundries.

Here, we present a two-dimensional scalable OPA on a Si PIC platform wherein each individual antenna element has its own ultralow power phase shifter consisting of an overcoupled ring resonator. The resonator phase shifters in this work are tuned using Si-doped microheaters integrated in close proximity to the resonators. With an 8×8 OPA with overcoupled ring resonator phase shifters, we demonstrate beamforming and beam steering, verify the low power consumption required for each application, and show the promise of this technology as a compact and low power on-chip SLM. Compared with our previously demonstrated work on

one-dimensional OPA using micro-ring resonators as phase shifters,[18] this work has increased the dimensionality of the OPA to two dimensions to enable two-dimensional beamforming and steering and has largely decreased the phase shifter power required for beam steering with much faster microheater tuning.

PIC-OPA DESIGN

Our PIC-OPA device is designed for large two-dimensional scaling with minimal power consumption. Figure 1(a) shows the schematic of a portion of the PIC-OPA architecture, containing many unit cells and displaying the optical routing. Laser light enters the array through a waveguide, and using tap couplers, it is split into eight bus waveguides with equal optical power. For each bus waveguide, there are eight unit cells consisting of tap couplers to extract the light as input to each OPA unit cell, which is shown in Fig. 1(b). As shown in this figure, the laser signal after the tapped coupler is sent to a ring resonator phase shifter before feeding the antenna of the unit cell. The antenna design is grating-based and optimized for maximum radiation efficiency.[18] All tap couplers are designed such that the antenna elements receive equal intensities, a necessary design consideration to prevent brightness inhomogeneities in the far-field when beamforming and beam steering. The optical routing within the array is scalable to realize a 2D OPA with a large number
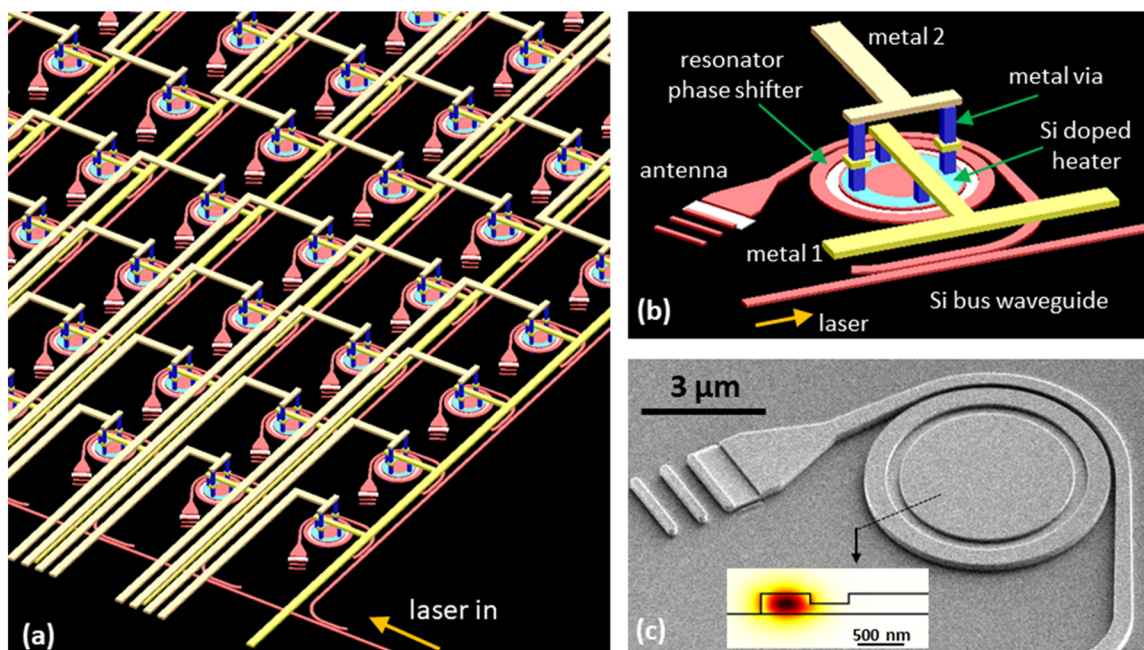
FIG. 1. PIC-OPA structure overview. (a) A schematic view of a portion of the 8×8 PIC-OPA designed for this work. Light enters the array through a waveguide, and using a tap coupler, it is split into eight bus waveguides with equal power. For each bus waveguide, there are eight tap couplers to extract the light and pass it to a ring resonator phase shifter before feeding it into an antenna. All tap couplers are designed such that the antenna elements receive equal intensities. (b) Schematic of a unit cell of the PIC-OPA. Laser light is tapped from a Si waveguide, goes through a strongly overcoupled ring resonator phase shifter ($\sim 3~\mu$m external radius), and then is sent to the antenna for radiation. The interior of the ring resonator is doped to create a resistive heater and has been segmented into four parallel resistor segments to reduce the overall resistance. Metal lines in two different layers connect these resistor segments and make them parallel. (c) A scanning electron microscope view of the unit cell before adding the metal contacts. The inset in (c) shows the cross section transverse-electric (TE) mode profile of the ring resonator.

of antenna elements.[1] An SEM of one unit cell on the device with the overcoupled ring resonator and antenna is shown in Fig. 1(c). Each unit cell is 15×15 μm^2 in size.

The ultralow power phase shifter is realized by Si-doped microheaters implemented in the interior region of the resonator, as shown in Fig. 1(b). The doped region, which is n-type, is segmented into four parallel resistor segments to reduce the overall resistance of the heater to sub-kΩ values. Two layers of metal contacts, as shown in Fig. 1(b), make these resistor segments parallel. A partially etched region separates the ring resonator region from the doped region. The purpose of this separation is to further confine the optical mode in the ring [see the inset of Fig. 1(c)] and minimize the optical absorption due to the doping region, which can degrade the resonator's intrinsic Q. The remaining silicon layer in the partially etched region allows efficient heat transfer from the heater to the optical mode of the ring.[19]

In this work, for proof of concept, we demonstrate an 8×8 OPA with 64 unit cells. Detailed design parameters are included in the supplementary material. In current array fabrication, the metal routing to all the phase shifters lies in the same optical layer [see Fig. 1(b)], limiting the array size. However, the architecture scales to larger sizes when electronic addressing is integrated under the optical layer.[20]

To enable a ring resonator to operate as a phase shifter, the coupling between the resonator and the external waveguide needs to be in a strong overcoupling regime. The transmission from a ring resonator can be derived as[18]

$$T = \frac{2i(\omega - \omega_0)/\omega_0 + 1/Q_0 - 1/Q_C}{2i(\omega - \omega_0)/\omega_0 + 1/Q_0 + 1/Q_C}, \tag{1}$$

where ω is the laser frequency, ω_0 is the resonant frequency of the resonator, Q_0 is the intrinsic quality factor of the resonator, and Q_C is the waveguide-resonator coupling quality factor. In the overcoupled regime, $Q_c/Q_0 \ll 1$, and in this case, the resonator phase is dependent on the coupling quality factor and is approximately equal to[18]

$$\phi \approx -2 \tan^{-1} \frac{2Q_C(\omega - \omega_0)}{\omega_0}. \tag{2}$$

Figure 2 shows the transmission intensity and the phase spectrum of a ring resonator coupled to a waveguide for different coupling regimes. As shown in Fig. 2(b), once $Q_c/Q_0 < 1$, the resonator can provide a 2π phase shift when sweeping the wavelength across its spectrum. However, in the strong overcoupling regime ($Q_c/Q_0 \ll 1$), the amplitude modulation for transmission is minimal, as shown in Fig. 2(a), providing a phase shifter with minimal amplitude distortion and a large phase shift. Such spectral response behavior with minimal amplitude distortion for the resonator and large 2π phase variation has already been employed in optical filter designs and is known as all-pass resonator filters.[21]

To achieve a strong overcoupling, careful design of the waveguide-resonator coupling is required. As shown in Fig. 1(b), we use a pulley coupling scheme to create a long interaction length between the waveguide and the resonator. In addition, the waveguide width and the gap between the waveguide and the resonator are designed to provide maximum phase matching and efficient
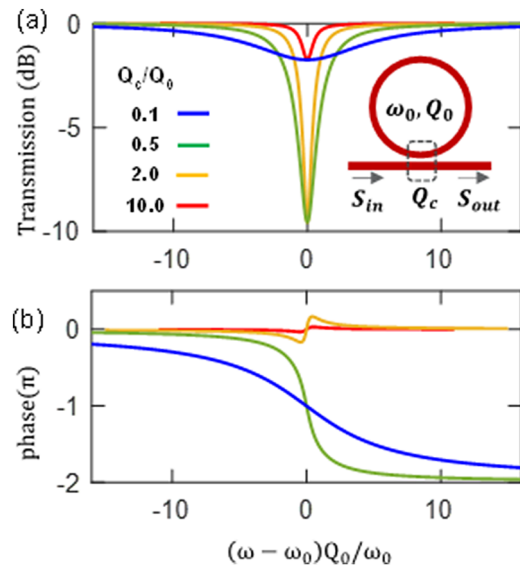
FIG. 2. Ring resonator as a phase shifter: (a)–(b) Transmission and phase spectrum of a waveguide coupled to a ring resonator for different coupling strengths in the undercoupled ($Q_c/Q_0 > 1$) and overcoupled ($Q_c/Q_0 < 1$) regimes. The inset in (a) shows the general schematic of the waveguide and resonator with resonance frequency (ω_0), intrinsic Q (Q_0), and coupling Q (Q_c). A strong overcoupled regime (e.g., $Q_c/Q_0 = 0.1$, blue plot) provides a large phase change with almost 2π phase variation when sweeping the laser and resonance frequency relative to each other and with minimum amplitude distortion of the transmission.

modal overlap between the waveguide mode and the resonator mode.

RESULTS

Our PIC-OPA is fabricated in a commercial silicon foundry. We designed all the devices in this OPA for a transverse electric (TE) polarization (see the supplementary material, Sec. S1). Figure 3(a) shows a microscope image of the 8×8 OPA device, while Fig. 3(b) shows a near-field image of light emitted from the OPA when a laser light (near 1550 nm) is coupled to the chip. As seen from this figure, all of the antennas have relatively uniform intensity.

Figure 3(c) shows the spectrum of a representative resonator phase shifter over a broad spectral range, wherein three resonances have been highlighted. The resonance near 1509 nm shows a strongly overcoupled resonance with a small transmission extinction of only ~0.5 dB and a resonance linewidth of ~450 pm. We use this resonance wavelength for beamforming and steering.

The resonator phase shifters, which are controlled by doped Si microheaters, are high speed and consume low power. The microheaters have a resistor value of ~400 Ω. Figure 3(d) shows the resonance shift of the phase shifters vs the applied voltage. In one case, we apply voltage to all 64 phase shifters to see the impact of the thermal crosstalk, and in the other case, we apply the voltage to only one of the phase shifters. We observe that by applying ~0.6 V to each microheater, we obtain a large 1.1 nm resonance shift, much larger than the resonance FWHM (0.45 nm). This demonstrates that
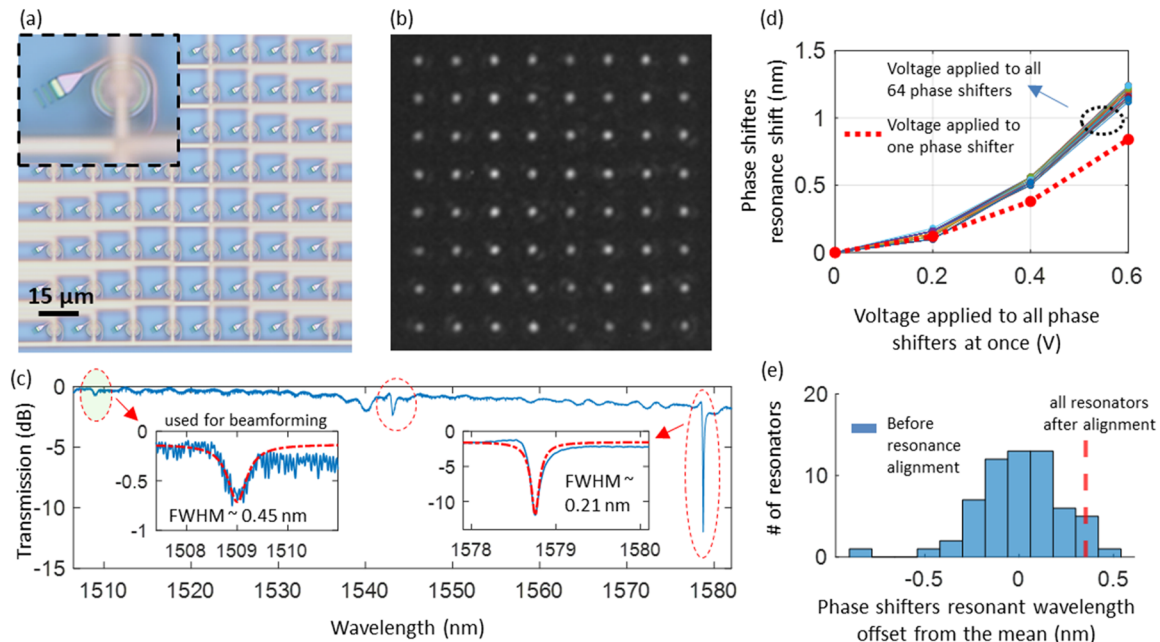
FIG. 3. (a) A microscope view of the OPA, with a zoomed-in view in the inset. Each unit cell of the OPA is $15 \times 15 \ \mu m^2$. (b) The measured near-field intensity of the OPA near 1550 nm, showing uniform intensity across the array. (c) A representative phase shifter resonance spectrum, wherein three of the resonances have been highlighted and show different levels of extinction. The right resonance has a larger extinction and narrower linewidth (FWHM ~0.2 nm), while the most left resonance is in the strongly over-coupled regime, i.e., shallow (~0.5 dB) extinction, and with an FWHM ~0.45 nm (see the supplementary material, Sec. S2). We use this resonance for far-field beam forming and steering. (d) Resonance shift of all 64 phase shifters vs the applied voltage. (e) Statistical variation of the untuned resonance wavelengths of all the resonator phase shifters within the 8×8 PIC OPA. This variation is due to fabrication imperfections. The dashed red line is the value at all the resonance wavelengths that are tuned to and lined up by applying a voltage to the microheater phase shifters. The resonance shift due to the heat power is ~1.1 nm/mW.

at low powers, we can have a ~2π phase shift when tuning the resonance around its center frequency [see Fig. 2(b)]. In addition, these microheater phase shifters show a high-speed frequency response of ~330 kHz (see the supplementary material), enabling high-speed spatial light modulation and beamforming. The total optical loss of the system from the fiber to each nanoantenna output includes fiber-to-chip coupling loss (~3 dB), phase shifter insertion loss (~0.5 dB), and nanoantenna radiation efficiency (~55% or 2.6 dB). This results in a total loss of ~6 dB.

Though the resonator phase shifters are identical in design, the fabrication imperfections cause a variation and a statistical distribution of resonance wavelengths for all 64 resonators, as shown in Fig. 3(e). Hence, we need to align these resonances. For the resonance alignment, we use the resonances at ~1579 nm, as shown in Fig. 3(c), because these resonances have higher extinction, allowing easier notch detection. This alignment will automatically nearly align all the resonances of other wavelengths (~1509 nm) that we use for beamforming and steering (see the supplementary material, Sec. S3, for further details). Perfect alignment is unnecessary, as a genetic algorithm will be used in the final alignment step.

Since, in the thermo-optics effect, we cannot cool down the resonators to blue-shift the resonance, we do the static alignment of all of the resonance wavelengths near the most red-shifted resonance. From our experiments, the vertical dashed line in Fig. 3(e)

corresponds to the optimal alignment wavelength reference, wherein there is only one resonance on the right side of this dashed line. This alignment reference allows full range steering and beamforming while minimizing the overall phase shifter's power. We expect that by using a better fabrication process, we will achieve less resonance wavelength variation.

To achieve the desired far-field beam pattern, we program the phase of each of the 64 microresonator phase-shifters by optimizing the far-field beam patterns according to simulated reference patterns (see the supplementary material, Sec. S4, for details). The thermal crosstalk of the phase shifters is compensated for in our far-field beam optimization without crosstalk measurement. For our device, the maximum unambiguous steering range is $5.8°$, and the FWHM of the far-field beam patterns is $0.6°$.

We achieve beamforming and steering with a low average power of ~300 μW per resonator phase shifter, where most of this power consumption (~250 μW) is static (bias), i.e., to align the resonance frequency of the resonators deviated by fabrication imperfections. The difference between total power and static power is ~50 μW and is the average of the elementwise resonator powers required for 16 evenly spaced beam steering positions. For the entire chip of 64 resonators, the dynamic power required for steering during the entire beam-steering process is thus ~3.2 mW. Figures 4(a) and 4(c) show the simulated far-field pattern and the corresponding
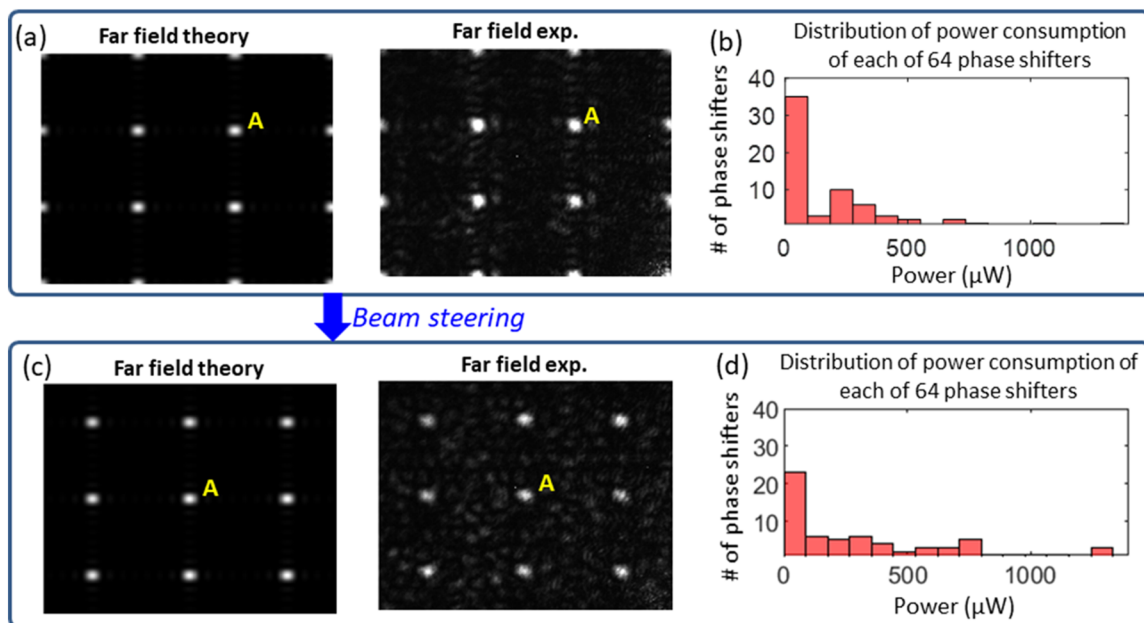
FIG. 4. Far-field beam forming and steering. (a) Simulated and experimental far-field for steering angles of $\phi_x = 0$, $\phi_y = 0$. For this device, the maximum unambiguous steering range is 5.8°, and the FWHM of the far-field beam patterns is 0.6°. (b) The power consumption range of the phase shifters for the far-field in panel (a). (c) and (d) Repeat the experiment in panels (a) and (b) but for steering phases (angles) of $\phi_x = \pi$ (2.9°) and $\phi_y = \pi$ (2.9°). One of the beam spots has been labeled with the letter **A** to clearly show its displacement in both horizontal (to the left) and vertical (to the down) when comparing panels (a) and (c). For all the beamforming and steering experiments, the average electric power consumption per phase shifter is ~300 μW, wherein 250 μW is static for the resonance alignment and 50 μW is dynamic for beamforming and steering. See also the supplementary material movie (Multimedia view) that shows steering for different angles and phases beyond π.

experimental results for two different beamforming points. We have labeled one of the far-field beam spots by the letter A in Figs. 4(a) and 4(c) to show where the beam moves. After calibration, the beam can be steered to any desired point in the far field [see the supplementary material movie (Multimedia view)].

For the optimization of the far-field beam patterns, we utilize two techniques in series (see also the supplementary material, Secs. S3 and S4). First, we process the phased arrays in the near-field using a swept source to extract the resonance spectra of the resonator phase shifters. Using a tunable laser, we sweep the laser wavelength while monitoring the radiated near-field intensity of each antenna via imaging and extract the corresponding phase shifter spectrum. After this measurement and identifying the resonances, we align all the resonance wavelengths by applying a voltage to the phase shifters and recording a lookup table of voltages that align all the resonances. From this point, we use a genetic algorithm to optimize the far-field beam pattern and find lookup tables of voltages for different beam locations. Gradient-based search algorithms and variants are a popular choice for optical phased array optimization and calibration,[22–25] though calibration can also be achieved analytically.[26] Figure 4(b) as well as Fig. 4(d) show the statistics of the power consumption of each phase shifter within the array for the corresponding far-field beams shown in panels (a) and (c). The average power for each phase shifter is less than 300 μW for all the steering angles within the 0-π phase shift, while about ~250 μW is static for the resonance alignment and ~50 μW is for beam forming,

more than one order of magnitude lower than all prior OPA works based on waveguide-based thermo-optic phase shifters [e.g., Refs. 1, 3, 9–11, and 15].

We also demonstrate the ability of the PIC-OPA with resonator phase shifters as a programmable SLM device to project arbitrary images into the far field. Figures 5(a) and 5(b) show the simulated and experimental demonstration of projecting the letter "R" in the far field as a proof of concept. Far-field pattern formation resolution is limited by the number of array elements. The beamforming quality is also limited by aberrations and undesired stray light scattering in the optical setup, which reduce the identicality between each periodic pattern in the far field. As shown by simulation in Figs. 5(c) and 5(d), with increasing the number of array elements, a higher resolution for the far-field patterns is achievable.

One important characteristic of the resonator phase shifter is its optical power handling before causing nonlinear distortion in the resonator spectrum due to two-photon absorption (TPA), TPA-induced free-carrier generation, and self-heating.[27,28] We characterize the resonator phase shifters at different laser powers and find that up to an on-chip laser power of ~1 mW in the waveguide before entering the resonator, the resonator spectrum remains almost unchanged (see the supplementary material section for more details). This level of laser power per phase shifter is quite sufficient when going to larger scale phased arrays, e.g., 128 × 128, as the total radiation power from the array can be several Watts. For the SLM application of this OPA, where the laser power is typically small,
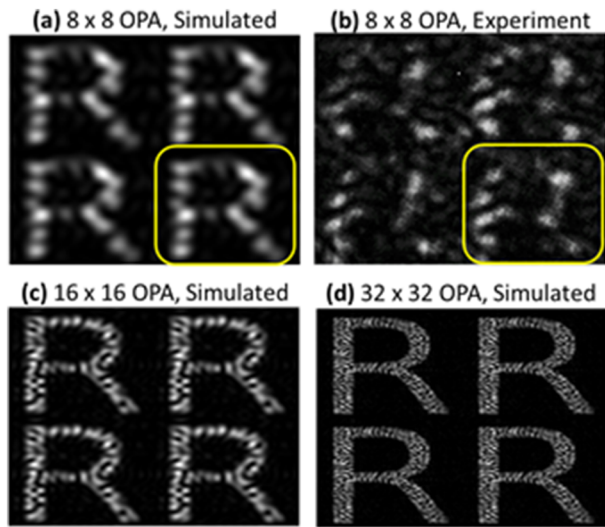
FIG. 5. Far-field pattern writing. (a) Simulated far-field of the 8 × 8 OPA for four repetitions of the letter R. (b) Experimental measured data corresponding to the simulated data in (a). One of the R letters has been highlighted with a yellow rectangle in panels (a) and (b) for a clear comparison of theory vs experiment. The lower image resolution in (a) and (b) is due to the small size of the OPA (i.e., 8 × 8). The panels in (c) and (d) show the simulated far field for a larger array with 16 × 16 and 32 × 32 elements with a higher image resolution.

we expect to use a laser power per phase shifter at the microwatt level.

In this work, we use a thermo-optics approach and use micro-heaters for the alignment and programming of the resonator phase shifters because the thermo-optics effect is quite strong with negligible optical loss. Though the electric power consumption for the individual resonance phase shifters is small, going to very large scale OPA (e.g., >256 × 256) will make the power management challenging. Most of the electric power consumption (~250 μW) is used for the resonance alignment of the resonators that are initially misaligned due to fabrication imperfections. With an improvement in the lithography and the fabrication process, we expect less resonance misalignment and lower electric power consumption by at least a factor of two. A narrower linewidth resonance can also reduce the dynamic power consumption of the phase shifters. The alternative phase shifting mechanism using PN junction charge depletion, though consuming low power (2), cannot provide large resonance shifts (e.g., ~ 1 nm) for the alignment of the resonators without sacrificing the intrinsic Q of the resonators. The doping of the resonator's optical region for efficient phase shifting will lower the intrinsic Q of the resonator (e.g., 10 000), making a strongly overcoupled design resonator with a finite loaded linewidth challenging. An alternate design is a hybrid approach employing both thermo-optics, as described here, and the PN junction approach, where the former is used for the resonators' resonance alignment and coarse programming and the latter for the fine wavelength tuning and programming of the OPA for beam forming.

The phase shifter's high speed (~330 kHz; see the supplementary material) has been enabled by the close proximity of the Si doped heater in the interior region of the resonator mode as well as efficient heat transfer from the doped heater to the resonator mode via the silicon device layer. This speed is dominantly limited by the large 2 μm thickness of the SiO$_2$ BOX layer, causing a larger value for the thermal resistance, which is inversely proportional to the heater's speed. Nevertheless, a thick SiO$_2$ BOX layer is essential to reduce thermal crosstalk between the adjacent phase shifters. A future work to further improve the phase shifter speed can be a hybrid design including both PN junctions and Si doped heaters in the resonator, as described earlier. The doped heater is used for coarse tuning and the PN junction for fast (~GHz) but finer wavelength range tuning. Since the PN junction phase shifter operation requires N and P dopants in the optical mode region of the resonator, such a hybrid design requires careful optimization of the doping level to not strongly reduce the resonator's intrinsic Q due to dopants and free carriers.

For the OPA devices in this work, we used an array pitch of 15 × 15 μm^2. While for beam steering applications, a smaller pitch is desired to increase the steering range, for the SLM application of the PIC-OPA, large pitch sizes are forgivable. Moving the electronic integration below the optical layer, as discussed earlier, can also assist in decreasing the unit cell size in future micro-ring resonator OPA designs. Future work on designing a more optimal antenna and a more compact resonator can further shrink the pitch. We expect a pitch as small as 9–10 μm to be possible. For the devices in this work, we used a periodic array, though, in principle, we can design a random sparse array[11,29] to suppress the side lobes and increase the steering range for the beam steering applications. A random sparse array design will also allow for large spacing between the array elements because the randomness and aperiodicity of the array will suppress the sidelobes that would have occurred due to the periodicity and large pitch.

CONCLUSION

In this work, we have demonstrated a silicon photonic 2D OPA as a low power programmable SLM with far-field beamforming and steering. Our PIC OPA consists of an 8 × 8 array with ultracompact and low power resonator phase shifters. With our 8 × 8 OPA, we perform beamforming and 2D beam steering as well as writing patterns in the far field. For these experiments, each phase shifter consumes an average of 300 μW of electric power, where most of it is static consumption to align the resonances due to fabrication imperfections. A future improvement in fabrication at a better foundry lithography node is expected to reduce the static power by at least a factor of two. Though in this work, we demonstrate a 2D OPA with periodic pixels, one can place antennas in random locations with an appropriate design algorithm to enable a random sparse array.[11]

Larger scale versions of our PIC-OPA SLM device with more array elements can be achieved by implementing electronic integration in a secondary layer below the optical layer. In addition, and for further scalability, one can form a super array composed of our OPA blocks, wherein optical signals are routed between these blocks. Our architecture shows great promise for a new generation of compact and efficient programmable photonic processors by combining the unique properties of planar and free-space optics.

AUTHOR DECLARATIONS

Conflict of Interest

M. Soltani, J. Leatham, and A. Singh are involved in developing PIC-OPA at Raytheon.

Author Contributions

All authors contributed to all aspects of this work.

Michelle Chalupnik: Conceptualization (equal); Formal analysis (equal); Investigation (equal); Methodology (equal); Software (equal); Validation (equal); Visualization (equal); Writing – original draft (equal); Writing – review & editing (equal). **Anshuman Singh**: Investigation (equal); Resources (equal); Validation (equal); Writing – review & editing (equal). **James Leatham**: Conceptualization (equal); Funding acquisition (equal); Project administration (equal); Resources (equal); Supervision (equal); Validation (equal); Writing – original draft (equal); Writing – review & editing (equal). **Marko Lončar**: Investigation (equal); Project administration (equal); Resources (equal); Supervision (equal); Validation (equal); Writing – original draft (equal). **Moe Soltani**: Conceptualization (equal); Formal analysis (equal); Funding acquisition (equal); Investigation (equal); Methodology (equal); Project administration (equal); Supervision (equal); Visualization (equal); Writing – original draft (equal); Writing – review & editing (equal).

DATA AVAILABILITY

The data that support the findings of this study are available from the corresponding authors upon reasonable request.

REFERENCES

[1] J. Sun *et al.*, "Large-scale nanophotonic phased array," Nature **493**(7431), 195–199 (2013).

[2] C. V. Poulton, M. J. Byrd, P. Russo, E. Timurdogan, M. Khandaker, D. Vermeulen, and M. R. Watts, "Long-range lidar and free-space data communication with high-performance optical phased arrays," IEEE J. Sel. Top. Quantum Electron. **25**(5), 1–8 (2019).

[3] D. N. Hutchison *et al.*, "High-resolution aliasing-free optical beam steering," Optica **3**(8), 887–890 (2016).

[4] M. J. R. Heck, "Highly integrated optical phased arrays: Photonic integrated circuits for optical beam shaping and beam steering," Nanophotonics **6**, 93 (2017).

[5] I. Christen *et al.*, "An integrated photonic engine for programmable atomic control," arXiv:2208.06732 (2022).

[6] C. L. Panuski *et al.*, "A full degree-of-freedom spatiotemporal light modulator," Nat. Photonics **16**, 834 (2022).

[7] C. Peng, R. Hamerly, M. Soltani, and D. R. Englund, "Design of high-speed phase-only spatial light modulators with two-dimensional tunable microcavity arrays," Opt. Express **27**, 30669–30680 (2019).

[8] D. Pierangeli, G. Marcucci, and C. Conti, "Large scale Ising machines by spatial light modulation," Phys. Rev. Lett. **122**, 213902 (2019).

[9] S. Chung, H. Abediasl, and H. Hashemi, "A monolithically integrated large-scale optical phased array in silicon-on-insulator CMOS," IEEE J. Solid-State Circuits **53**(1), 275–296 (2018).

[10] S. A. Miller *et al.*, "Large-scale optical phased array using a low-power multi-pass silicon photonic platform," Optica **7**, 3 (2020).

[11] R. Fatemi, A. Khachaturian, and A. Hajimiri, "A nonuniform sparse 2-D large-FOV optical phased array with a low-power PWM drive," IEEE J. Solid-State Circuits **54**(5), 1200 (2019).

[12] W. Ma *et al.*, "Practical two-dimensional beam steering system using an integrated tunable laser and an optical phased array," Appl. Opt. **59**(32), 9985 (2020).

[13] Y. Guo *et al.*, "Integrated optical phased arrays for beam forming and steering," Appl. Sci. **11**, 4017 (2021).

[14] Y. Wang *et al.*, "2D broadband beam steering with large-scale MEMS optical phased array," Optica **6**(5), 557 (2019).

[15] F. Ashtiani and F. Aflatouni, "NxN optical phased array with 2N phase shifters," Opt. Express **27**, 27183 (2019).

[16] Y. Liu and H. Hu, "Silicon optical phased array with a 180-degree field of view for 2D optical beam steering," Optica **9**, 903–907 (2022).

[17] N. Dostart, B. Zhang, A. Khilo, M. Brand, K. Al Qubaisi, D. Onural, D. Feldkhun, K. H. Wagner, and M. A. Popović, "Serpentine optical phased arrays for scalable integrated photonic lidar beam steering," Optica **7**, 726–733 (2020).

[18] H. Larocque *et al.*, "Beam steering with ultracompact and low-power silicon resonator phase shifters," Opt. Express **27**, 34639 (2019).

[19] E. Timurdogan *et al.*, "An ultralow power athermal silicon modulator," Nat. Commun. **5**(1), 4008 (2014).

[20] K. Taehwan *et al.*, "A single-chip optical phased array in a wafer-scale silicon photonics/CMOS 3D-integration platform," IEEE J Solid State Circuit **54**, 3061 (2019).

[21] C. K. Madsen and J. H. Zhao, in *Optical Filter Design and Analysis: A Signal Processing Approach*, 1st ed. (Wiley, New York, 1999), Chap. 6.

[22] F. Aflatouni, B. Abiri, A. Rekhi, and A. Hajimiri, "Nanophotonic projection system," Opt. Express **23**(16), 21012 (2015).

[23] N. Nakamoto, T. Takahashi, Y. Konishi, and I. Chiba, "Phase optimization for accurate beam forming of phased array with element field errors at every phase shift," in *2013 IEEE International Symposium on Phased Array Systems and Technology* (IEEE, 2013), pp. 693–697.

[24] T. Komljenovic and P. Pintus, "On-chip calibration and control of optical phased arrays," Opt. Express **26**(3), 3199 (2018).

[25] F. Xiao, L. Kong, and J. Chen, "Beam-steering efficiency optimization method based on a rapid-search algorithm for liquid crystal optical phased array," Appl. Opt. **56**(16), 4585 (2017).

[26] B. V. Gurses, R. Fatemi, A. Khachaturian, and A. Hajimiri, "Large-scale crosstalk-corrected thermo-optic phase shifter arrays in silicon photonics," IEEE J. Quantum Electron. **28**(6), 6101009 (2022).

[27] P. E. Barclay, K. Srinivasan, and O. Painter, "Nonlinear response of silicon photonic crystal microresonators excited via an integrated waveguide and fiber taper," Opt. Express **13**, 801 (2005).

[28] M. Soltani, S. Yegnanarayanan, Q. Li, A. Eftekhar, and A. Adibi, "Self-sustained gigahertz electronic oscillations in ultrahigh-Q photonic microresonators," Phys. Rev. A **85**, 053819 (2012).

[29] T. Komljenovic, R. Helkey, L. Coldren, and J. E. Bowers, "Sparse aperiodic arrays for optical beam forming and LIDAR," Opt. Express **25**, 2511 (2017).

17 October 2023 09:14:52